Structural Engineering and Mechanics, *Vol. 62, No. 4 (2017) 455-464*
DOI: https://doi.org/10.12989/sem.2017.62.4.455

Effects of viscous damping models on a single-layer latticed dome during earthquakes

Huidong Zhang[*1,2a], Jinpeng Wang[1,2], Xiaoshuai Zhang[1,2] and Guoping Liu[1,2]

[1]*Tianjin Key Laboratory of Civil Buildings Protection and Reinforcement, No.26 Jinjing Road, XiQing District, Tianjin 300384, PR China*
[2]*School of Civil Engineering, Tianjin Chengjian University, No.26 Jinjing Road, XiQing District, Tianjin 300384, PR China*

(Received September 26, 2016, Revised November 28, 2016, Accepted March 9, 2017)

Abstract. Rayleigh damping model is recommended in the recently developed Performance-Based Earthquake Engineering (PBEE) methodology, but this methodology does not provide sufficient information due to the complexity of the damping mechanism. Furthermore, each Rayleigh-type damping model may have its individual limitations. In this study, Rayleigh-type damping models that are used widely in engineering practice are discussed. The seismic performance of a large-span single-layer latticed dome subjected to earthquake ground motions is investigated using different Rayleigh damping models. Herein a simulation technique is developed considering low cycle fatigue (LCF) in steel material. In the simulation technique, Ramberg-Osgood steel material model with the low cycle fatigue effect is used to simulate the non-uniformly distributed material damping and low cycle fatigue damage in the structure. Subsequently, the damping forces of the structure generated by different damping models are compared and discussed; the effects of the damping ratio and roof load on the damping forces are evaluated. Finally, the low cycle fatigue damage values in sections of members are given using these damping models. Through a comparative analysis, an appropriate Rayleigh-type damping model used for a large span single-layer latticed dome subjected to earthquake ground motions is determined in terms of the existing damping models.

Keywords: viscous damping model; single-layer latticed dome; fatigue; damping force; damage

1. Introduction

Seismic analyses were first developed for elastic structures. In an elastic time history analysis, damping is approximated at the global scale to represent all the dissipated energy in a structure. However, this approximation is generally not satisfactory for the large inelastic deformations of structures when strong earthquakes occur (Chopra 1995). It is because the energy dissipation sources, such as viscous, friction, and hysteretic devices, have to be adequately considered in a nonlinear dynamic analysis (Deierlein *et al*. 2010). For a convenient damping model, the simplest equation for damping force is (Vargas and Bruneau 2007)

$$F_d=-cv \tag{1}$$

where F_d is the damping force, c is the damping constant or damping coefficient, and v is the velocity of an object. The above equation is called viscous damping model, and it describes a typical case for an object that is dampened by a fluid at relatively low speeds. However, that is not the case for most building structures because the damping is not viscous, and the assumption for Eq. (1) is violated.

The actual damping in a structure is extremely difficult to be identified and the formulation of the damping force is very complicated. However, the classical viscous damping model (Rayleigh damping) is used widely in engineering practice. The Rayleigh damping formulation is as follows

$$[C]=\alpha_m[M]+\beta_k[K] \tag{2}$$

in which α_m and β_k are the mass–proportional damping coefficient and stiffness–proportional damping coefficient, respectively; [M], [K], and [C] are the mass matrix, stiffness matrix, and damping matrix, respectively. This model was originally developed in the linear-elastic dynamic analysis. In this model, the mass component dampens the energy at the low frequency domain, while the stiffness component dampens the energy at the high frequency domain. Evidently, the mass-proportional damping is difficult to be justified practically because the air damping is negligible for most structures (Hall 2006). However, mathematically it is very convenient because of its decoupling features. In fact, the internal friction is the most significant damping source in structures (Charney 2008, Filiatrault *et al*. 2002). Due to the presence of the friction damping, the damping ratios of a structure are almost frequency-independent and the structure exhibits hysteretic characteristics to a certain extent even within the elastic stage (Bernal 1994). In addition, there may be other damping that have not been studied, but they do not contribute considerably to total damping, such as radiation damping, which decreases with the decrease in frequency and the increase in slenderness. If the energy dissipation sources are not able to be directly modeled, Rayleigh damping can be used to represent the unknown energy dissipation at the structure level.

*Corresponding author, Professor
E-mail: zhhuidong@126.com

Copyright © 2017 Techno-Press, Ltd.

ISSN: 1225-4568 (Print), 1598-6217 (Online)

As described above, Rayleigh damping can be used as an additional energy dissipation source for the purpose of mathematical convenience. Therefore, Rayleigh damping model has to be carefully designed to avoid unintended consequences and to provide the best control in dynamic analyses (Bernal 1994). In recent years, researchers have investigated the limitations of Rayleigh damping when it is used for the inelastic systems, and some methods for practical references are proposed. Charney (2008) considered that although the mass-proportional damping is difficult to be justified physically, it provides an additional control on the modal damping ratios in finite element practice to avoid the numerical divergence. PEER/ATC (2010) pointed out that it is generally accepted that the stiffness-proportional term of the damping matrix should exclude or minimize the transition effect from elasticity to plasticity, in which stiffnesses change dramatically during dynamic analyses. Another suggested approach (Hall 2006) was to eliminate the stiffness-proportional damping term and to only specify a value for the mass–proportional damping term. However, as shown by Jehel and Léger (2014), researchers also recommended to use the Rayleigh damping models based on the initial stiffness. Zareian and Medina (2010) stated that excessive damping forces can be generated when the initial stiffness-proportional model was used, and they pointed out that the tangent stiffness-proportional damping model was recommended in engineering practice. Most existing guidelines (Deierlein *et al.* 2010, PEER/ATC 2010, ATC 1997, Kelly 2001) still suggest to use Rayleigh damping model, but do not provide sufficient information, such as the limitations and applications of different damping models for different building systems. In these guidelines and documents, Rayleigh damping models were modified. *NEHRP* (Deierlein *et al.* 2010) recommends that the reasonable periods, $0.2T$ and $1.5T$, are used to specify the damping values to calculate the damping coefficients, where T is the fundamental vibration period of the structure. In the user manual of the computer program *PERFORM-3D* (CSI 2007), the mass and stiffness damping coefficients are computed by means of $\omega_a=1.10\omega_1$ and $\omega_b=4.00\omega_1$. In SAC projects (Krawinkler 2000), the damping coefficients are defined by $\omega_a=\omega_1$ and $\omega_b=0.2$s. On the other hand, Charney (2008) suggested that the first frequency, ω_a, of a building should be expected to be reduced to $0.667\omega_1$ due to non-linear softening, and the second frequency, ω_b, can be set to $3\omega_1$. According to the above literatures, it is found that there is at present still no clear consensus on how to use Rayleigh damping in engineering practice. Although the viscous damping does not exist in real buildings, the damping in buildings can be approximated by the viscous damping formula even if there is no viscous material in structures (Tamura 2012). Therefore, it is necessary to further investigate the effects of these viscous damping models on dynamic demands when they are applied to engineering structures. This is one of objectives of this study.

In Rayleigh damping model, the definition of the damping coefficients depends on not only the circle frequencies of a structure but also its damping ratios. The uncertainty of the damping ratio leads to inaccurate dynamic predictions. In a nonlinear analysis, PEER/ATC (2010) suggests a minimum value, which is 2% of the critical damping. The increase of damping beyond this value depends on whether hysteretic energy dissipation in the structural components is explicitly captured. Existing guidelines (AISC 2005) suggest to use the viscous damping ratio that is less than 1% for large span space structures. Many codes also suggest that the damping values of about 1% be used to model the energy dissipation for steel frame structures under small deformations. Currently, the damping ratios are obtained based on the full-scale test data. Goel and Chopra (1997) found that the equivalent damping ratio for buildings in excess of 35 stories ranged between 2%-4% of the critical damping based on the data obtained from strong earthquake motions. By means of the full-scale test data of the buildings in Japan, the equivalent damping ratio of 1% to 2% in steel structures was observed (Satake *et al.* 2003). Tatemichi *et al.* (1997) collected the data from the vibration test of 33 dome-shaped structures in Japan; the results showed that the damping ratio of the first mode depended on both the vibration amplitude and the span length, and an approximate relationship between the first damping ratio and the length of the span was given by $\xi_1=0.03\times L/100$, in which L is the span length. The results of the wind tunnel tests on cable domes showed that the damping ratio increased with the increase in the wind speed, ranging from 2%-4% (Li *et al.* 2009), and it should be noted that these damping ratios were greatly influenced by friction damping. The experimental data on the damping are very limited due to the difficulty in obtaining enough test data, and they are not sufficient for giving a detailed description of the damping ratios for large domes. Therefore, the second objective of this study is to assess the sensitivity of the dynamic demands to the assumed damping ratios.

In the current study, a simulation technology is developed to simulate the nonlinear behaviors of members, and a large span single-layer latticed dome that is subjected to earthquake ground motions is investigated and compared using different Rayleigh-type damping models. Finally, the low cycle fatigue damage values in sections of members are given using these damping models.

2. Ramberg-Osgood steel material model with low cycle fatigue effect

2.1 Ramberg-Osgood steel material model

In this study, a material model is used for a large span single-layer latticed dome (Zhang *et al.* 2016) in order to accurately capture the steel material damping (Zhang *et al.* 2015). The Ramberg-Osgood (R-O) steel material model in OpenSees is presented herein. It describes a nonlinear hysteretic relationship between the stress and the strain showing a smooth elastic-plastic transition. This model is very useful for modeling the materials that harden with plastic deformation. In the field of earthquake engineering, the Ramberg-Osgood model is often used to simulate the behavior of structural steel materials and components

(Mazzoni *et al.* 2004). The model is mathematically expressed as (Ramberg and Osgood 1943)

$$\varepsilon=\frac{\sigma}{E}+K(\frac{\sigma}{E})^n \tag{3}$$

where ε is the strain, σ is the stress, and E is the modulus of elasticity. K and n are constants, describing the hardening behavior of the material. By introducing the yield strength of the material σ_0 and defining a new parameter α, here, $\alpha = K(\sigma_0/E)^{n-1}$, it is convenient to rewrite the second term on the right-hand side as

$$K(\frac{\sigma}{E})^n=\alpha\frac{\sigma_0}{E}\left(\frac{\sigma}{\sigma_0}\right)^n \tag{4}$$

The expression $\alpha\frac{\sigma_0}{E}$ can be treated as a yield offset. The value of α can also be found by means of experimental data. According to metallic material experiments, it is observed that the yield offset is equal to 0.2%. Therefore, Eq. (3) is further expressed as

$$\varepsilon=\frac{\sigma}{E}+0.002(\frac{\sigma}{\sigma_0})^n \tag{5}$$

Through the experimental tests, it is recommended that the parameter n should be approximately equal to 8~10 for common steel material (Sheen 1984). The stress-strain relationship of the Ramberg-Osgood model shown in Eq. (5) includes the elastic part and plastic part. Different parameters lead to different stress-strain curves during loading and unloading, and this difference is caused by the internal friction of the material. As a result, compared with other bi-linear material models, this steel constitutive model can explicitly model the material damping even within the elastic region. Moreover, the formula of the Ramberg-Osgood model given by Eq. (5) is also adopted by the American Society of Civil Engineers (ASCE) design specification (ASCE/SEI 2003).

2.2 Modeling of fracture due to low cycle fatigue

2.2.1 Low cycle fatigue model

In this study, the material fatigue effect in a large span single-layer latticed dome is considered. The relevant investigation (Shemshadian *et al.* 2011) on various damaged structures subjected to earthquakes shows that the structural failures are related to the damage caused by the cumulative effects of a few cycles of high strain amplitudes. This type of failure is termed as "low cycle fatigue" (LCF). The conventional plasticity constitutive models that are used in the simulation of the structures normally do not address the fatigue damage, and LCF is not explicitly mentioned in the seismic design standards (AISC 2005). However, as stated by Lignos *et al.* (2011), the effects of fatigue damage on the structural components may become critical for structural design because of the large number of load cycles. In the recently developed Performance-Based Earthquake Engineering (PBEE) methodology, the evaluation and assessment on the fatigue damage are considered. Moreover, several structural cumulative damage models during earthquakes have been proposed (Mehanny and Deierlein 2001, Hindi and Sexsmith 2001, Park and Ang 1985, Stephens *et al.* 2000). Among these models, the Coffin-Manson law is widely used to simulate the mechanical fatigue damage of steel material. The Coffin-Manson law is expressed as (Stephens *et al.* 2000)

$$\varepsilon_i = \varepsilon_0(N_f)^m \tag{6}$$

where ε_0 is the fatigue ductility coefficient, which roughly indicates the strain amplitude at which one complete cycle on a virgin material causes failure; m is the fatigue ductility exponent, which describes the sensitivity of the strain amplitude to the number of cycles leading to failure; N_f is the number of constant amplitude cycles leading to failure and ε_i is the strain amplitude experienced in each cycle. In the Coffin-Manson law, a linear relationship is assumed between the log of N_f and the log of ε_i. For the cumulative damage under the stress cycles with varying magnitudes, the Palmgren-Miner linear cumulative fatigue damage theory (Miner's Rule) is used to calculate the damage value (Mazzoni *et al.* 2004). According to the Rule, the index of damage D is as follows

$$D = \sum\frac{n_i}{N_{fi}} \tag{7}$$

where n_i and N_{fi} are the applied cycle number under the i^{th} constant amplitude loading and total cycle number leading to failure, respectively. In Eq. (7), D is a parameter that varies from 0 at undamaged state to 1 at fatigue failure. The stress of an element becomes zero when the fatigue life is exhausted. In Eq. (6), the fatigue ductility coefficient and exponent can be calibrated by low cycle fatigue tests. For wide flange beams, the typical values are m=-0.458 and ε_0=0.191 (Mazzoni *et al.* 2004), while these values are m=-0.5 and ε_0 =0.095 for hollow structural sections (Uriz 2005). Based on the low cycle fatigue tests for the austenitic stainless steel AISI 303, it is observed that the fatigue ductility coefficient and exponent are m=-0.292 and ε_0=0.052, respectively (Anes *et al.* 2014). In most general situations, the material is subjected to complex fatigue loading conditions that generate the multi-axial stress states, and the material easily fatigues. Using a smaller value of ε_0 than required, it may provide an appropriate prediction.

The material constitutive model presented in Fig. 1, which combines the R-O model with the fatigue effect shown in Fig. 2, is implemented in OpenSees. Here, it is assumed that the fatigue properties is similar to austenitic stainless steel AISI 303, and the fatigue ductility coefficient and exponent are set as m=-0.29 and ε_0=0.05, respectively. It should be noted that the fatigue material model wraps around R–O steel material in OpenSees and does not influence the stress–strain relationship of the parent material, and the damage value and fracture behavior of the material can be computed and captured by this model.

2.2.2 Hysteresis of a tubular member

In a single-layer latticed dome, the members are mostly subjected to large axial loads and a small amount of end moments (Zhang and Han 2013, Zhang and Wang 2015). The members with large slenderness ratios are easier to lose stability under cyclic loads. Although the failure of an individual member does not necessarily lead to an overall structural collapse, it causes the internal force redistribution in the members, and ultimately reduces the loading capacity of the dome. During the last decade, the overall and local buckling behaviors of cylindrical tubular members have been intensively investigated. Gupta *et al.* (1993, 2004) pointed out that the loading capacity, deformation and failure mode of thin tubes depend on the diameter-to-thickness ratio, material constitutive model, initial geometrical imperfection, and constraint conditions of a member. Teng (1996) considered that the theoretical buckling load based on the assumption of a perfect geometry shape significantly overestimates the actual strength of a thin steel tube. Therefore, the initial imperfection, such as the initial deflection, has an important effect on the loading capacity of a thin tubular member. Here, a tubular member (the cross sectional diameter Di=355.6 mm and wall thickness t=6.3 mm) with the length 5.64 m and initial deflection d=0.0564 m is investigated to present the loading capacity under cyclic loading using the OpenSees software, as shown in Fig. 3. The tubular member is modeled as two *Displacement-Based Beam-Column* elements. The ends of the tube are connected with the elastic members in order to model the constraint conditions. The stiffnesses of the elastic members are far larger than that of the tube, and each elastic member is modeled as two *elasticBeamColumn* elements.

Fig. 4 shows the hysteretic response of the tube under varying axial loads. It is observed that the ductility of the tube with the imperfection under compression is lower than that under tension. The loading capacity decreases with the increase in the cycles and the strength deterioration occurs. The loading capacity under compression is less than that under tension. As a result, the backbone curves (the dot curves in Fig. 4) under the compression and tension states are asymmetric. However, if without this initial deflection, the tube will behave as an ideal member without a global buckling. It is because a small initial imperfection can initialize a deviation and overall buckling of the member.

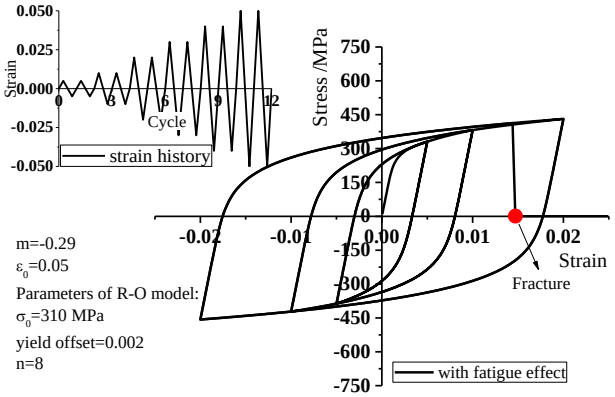

Fig. 1 R-O material with fatigue effect

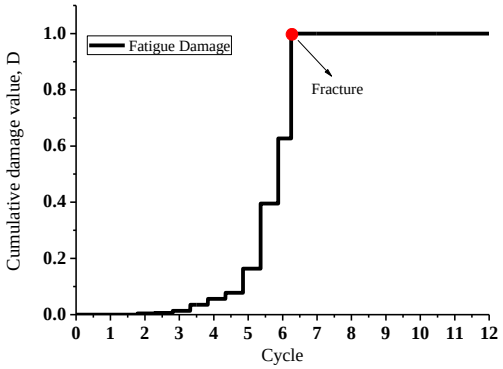

Fig. 2 Fatigue damage value of material

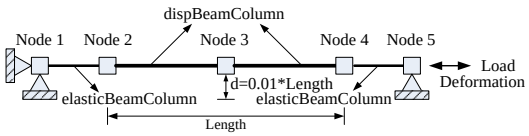

Fig. 3 Mechanical model of tubular member

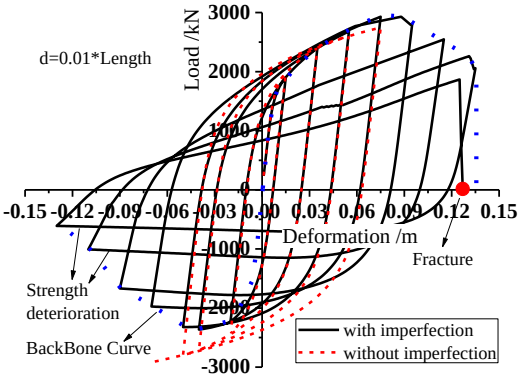

Fig. 4 Hysteretic response of tubular member

3. Numerical example

3.1 Model description

A single-layer latticed dome with welded ball joints is considered in this study, as shown in Fig. 5. Its span length is 100 m and the height is 22.22 m. The span-rise ratio is 4.5.

In the model, the elastic modulus and yield strength of the steel material are 200 GPa and 310 MPa, respectively. In this study, the hardening parameter and yield offset are set as 8 and 0.2% for the Ramberg-Osgood steel material, respectively. The used members are steel tubes and the section sizes are listed in Table 1. The uniform roof load is 180 kg/m^2, and it is assumed to be concentrated at the joints as masses. OpenSees software is used to develop the 3D model of the dome. The *Displacement-Based Beam-Column* element with a distributed plasticity and linear curvature distribution is used to model the nonlinear behaviors of the members. The geometric nonlinearity is also considered in this study. Each member is modeled as one element and each element has five integration points along the element length to evaluate the dynamic response of the element. The section of each tube is dispersed into 16 fiber areas.

Through an eigenvalue analysis, the dynamic characteristics of the dome are shown in Table 2. According to Table 2, it is observed that the first ten frequencies are very close to each other, therefore, a step-by-step integration method for the dynamic analysis of this kind of structural system is more effective than a mode superposition method due to the mode coupling.

The earthquake loads with different hazard levels from the PEER strong ground motion database are applied to the structure, as listed in Table 3. These seismic loads are applied after the gravity loads.

Table 1 Section sizes of the single-layer latticed dome

Member	Hoop member	Ridge member	Diagonal member	Tension member
Size	Φ355.6×8 mm	Φ355.6×6.3 mm	Φ355.6×6.3 mm	Φ700.0×14.0 mm

Table 2 Frequencies of the single-layer latticed dome (roof load 180 kg/m^2)

Mode	1	2	3	4	5	6	7	8	9	10
Frequency /(rad/s)	13.80	13.80	15.06	15.06	15.28	15.32	15.35	15.39	15.47	15.51

Table 3 Three earthquake ground motion records

Earthquake ground motions	*PGA/g*			*Duration*	*Scale factor*
	x	*y*	*z*		
Tabas, Iran 1978/09/16 (9102 Dayhook)	0.406	0.328	0.183	23.84s	1
Victoria, Mexico 1980/06/09 (6604 Cerro Prieto)	0.621	0.587	0.304	24.45s	1
Northridge 1994/01/17 (24087 Arleta)	0.344	0.308	0.552	40s	1

Table 4 Damping models for dynamic analyses

	Damping models	Damping coefficients
Model 1	Mass-proportional damping, $\alpha[M]$	$\alpha=2\xi_1\omega_1$
Model 2	Initial stiffness-proportional damping, $\beta[K]$	$\beta=2\xi_1/\omega_1$
Model 3	Tangent stiffness-proportional damping, $\beta[K_t]$	$\beta=2\xi_1/\omega_1$
Model 4	Rayleigh damping, $\alpha[M]+\beta[K]$	$\alpha=2\xi_1\omega_i\omega_j/(\omega_j+\omega_i)$; $\beta=2\xi_1/(\omega_j+\omega_i)$
Model 5	Rayleigh damping, $\alpha[M]+\beta[K]$	$\alpha=2\xi_1\omega_i\omega_j/(\omega_j+\omega_i)$; $\beta=2\xi_1/(\omega_j+\omega_i)$ ($\omega_i=0.667\omega_1$, $\omega_j=3\omega_1$)
Model 6	Rayleigh damping, $\alpha[M]+\beta[K]$	$\alpha=4R\xi\omega_i/(1+R+2R^{0.5})$; $\beta=4\xi/[\omega_i(1+R+2R^{0.5})]$ ($R>1$) ($\omega_i=0.667\omega_1$)

3.2 Viscous damping models

According to Tatemichi *et al.* (1997), the equivalent viscous damping ratio of the first mode of the dome is about 0.03. The damping ratio of the high mode is also assumed as 3% in order to define the damping coefficients. For a parametric study, the damping ratios are selected as 1%, 3%, and 5%, respectively. The damping models selected are listed in Table 4, which are widely used in dynamic analyses. In models 1-3, the first damping ratio and circle frequency are used to determine the damping coefficients. For model 4, the classical Rayleigh damping model is used, and the first and third circle frequencies are selected to determine the mass and stiffness damping coefficients, respectively. While model 5 proposed by Charney (2008) takes the soft effects of the structure into account due to yielding, in which ω_i and ω_j are set as $0.667\omega_1$ and $3\omega_1$, respectively. Model 6 that was proposed by Hall (2006) is more sophisticated, in which the bound Δ on the damping ratios within the specified frequency is determined by the following equation

$$\Delta=\xi\frac{1+R-2\sqrt{R}}{1+R+2\sqrt{R}} \tag{8}$$

where $R>1$. If the bounds are considerably narrow, the damping coefficients can be fixed by the equations in model 6. The frequency range is from ω_i to $R\omega_i$ in model 6. Here, R is set as 1.7 for the dome and it ranges from 9.21 rad/s to 15.66 rad/s, which includes the first ten mode frequencies.

Fig. 6 depicts the different viscous damping models used in this analysis. These viscous damping models have a

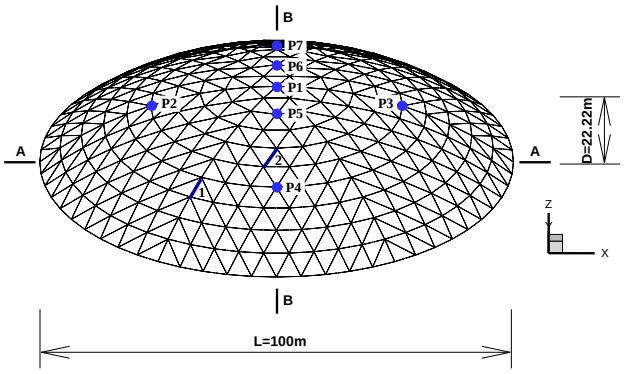

Fig. 5 A typical large span single-layer latticed dome

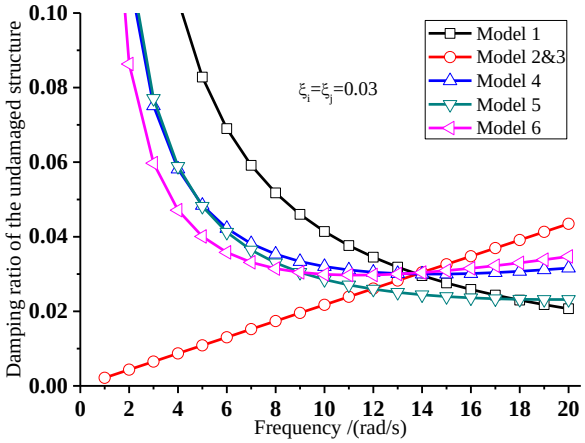

Fig. 6 Damping ratio vs frequency curves of models

similar characteristic, and it is that the damping ratio is only frequency-dependent regardless of the structural systems. In the figure, it shows that models 4, 5, and 6 have a near-constant damping ratio within the elastic range, whereas the difference can be observed. However, the damping ratio in model 1 decreases with the increase in the frequency, and the damping ratios of models 2 and 3 increase with the increase in the frequency. Among these models, model 5 provides relatively small structural damping ratios within the elastic range, while models 2 and 3 provide relatively large structural damping ratios within the elastic range. It should be noted that the modal properties of damaged structure in Fig. 6 are only assumed to define the damping coefficients α and β and there is no shift of modal properties between the undamaged structure and the damaged structure. The damping model with the moderate damping effect should be a good option among these damping models because it is important to make sure that the damping forces generated by the uncertain viscous damping models is kept at an appropriate level, and the errors of the damping forces in the dome may be the smallest in this case. Therefore, the effects of these damping models on the damping forces should be quantified and discussed to find the appropriate viscous damping model for the dome.

4. Results

4.1 Response analysis

4.1.1 Effect of the damping model on the response

In the current earthquake performance-base and assessment methodology, the peak displacement is a critical parameter. Fig. 7 represents the vertical peak displacements at the top of the dome. It shows that the use of the damping models 2 and 3 leads to the smaller response, whereas model 1 gives the maximum peak demand. The clear difference is observed due to the use of different damping models. This can be explained as follows. For model 1 (the mass-proportional damping model), the damping ratio decreases with the increase in the frequency, and the higher-mode effect on the seismic behavior of the dome is noticeable due to the low damping ratio. Compared with other models, the use of model 1 reduces the damping effect in the dome. For models 2 and 3 (the stiffness-proportional damping model), the damping ratio increases with the increase in the frequency, and the contribution of the higher-mode to the dynamic response will be dampened due to the high damping ratio. It is also found that the difference between the initial stiffness-proportional damping model and the tangent stiffness-proportional damping model is not significant. While models 4, 5, and 6 have the moderate damping effects on the dome, and the responses are among models 1, 2, and 3.

4.1.2 Effect of the damping ratio on the response

Damping ratio is an important dynamic factor in controlling the structural response. In this study, the single-layer latticed dome with a roof load of 180 kg/m^2, which is subjected to Victoria (Mexico, 1980) earthquake ground motion, is investigated.

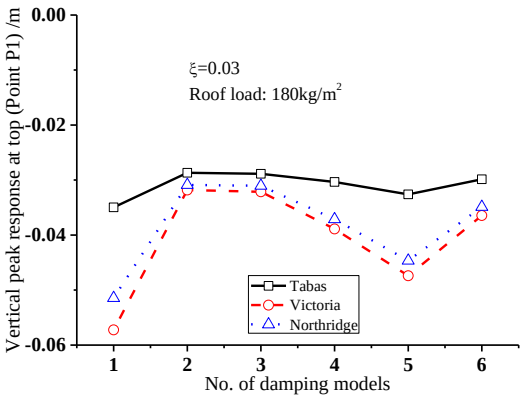

Fig. 7 Vertical peak deformations under different models

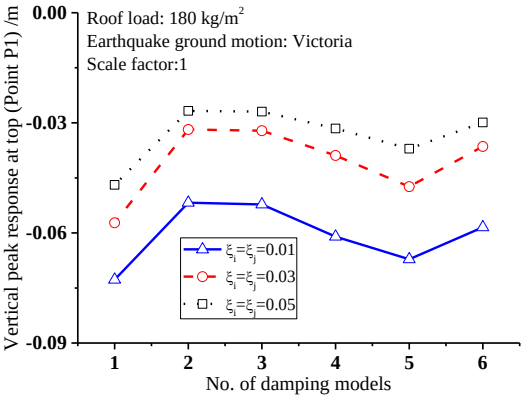

Fig. 8 Vertical peak displacements at top

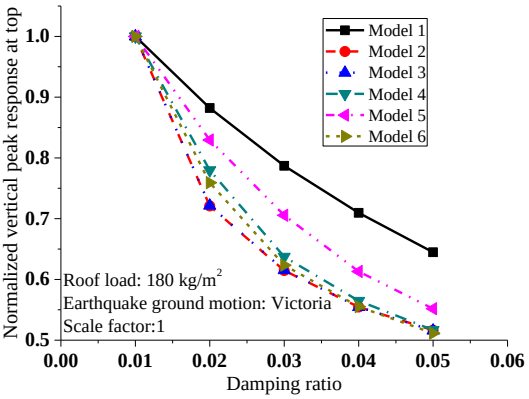

Fig. 9 Normalized vertical peak displacements at top

Fig. 8 shows the vertical peak deformations under the damping ratios of 1%, 3%, and 5%. It indicates that the damping ratio has a significant effect on the response. The peak response remarkably decreases with the increase in the damping ratio. This observation may be a crucial issue in the earthquake performance-base assessment because the overestimation of the damping ratio not only underestimates the dynamic response, but also overestimates the earthquake performance of the structures, which is not conservative for structural safety. Although the underestimation of the damping ratio can lead to the non-conservative dynamic response, more members have to be used in this case and

this increases the construction cost in order to ensure the structural safety. Therefore, the selection of an appropriate damping ratio can not only accurately predict the structural seismic performance, but also limit the cost at an appropriate level.

With the increase in the damping ratio, the effect of each viscous damping model on the efficiency in controlling dynamic response is different, which is of particular concern in structural engineering. Fig. 9 represents the changing trends in the normalized vertical peak responses under damping ratios ranging from 1% to 5%. It should be noted that the peak deformations of models 2, 3, 4, and 6 rapidly decrease with the increase in the damping ratio, therefore, these models have a larger inhibiting effect on the peak responses as compared to the model 1. It is also observed that the sensitivity of model 5 to the damping ratio falls in between these models. In model 5, the peak deformation of the structure with damping ratio 5% is around 0.55 times that of the structure with the damping ratio 1%.

4.2 Viscous damping force

4.2.1 Effects of the damping models on the viscous damping force

In this study, a comparison on the damping forces of joints is made for better understanding the damping forces generated in the dome. Figs. 10 and 11 represent the mean values of the vertical peak damping forces of the joints of Sections A-A and B-B (Fig. 5) under all earthquake ground motions.

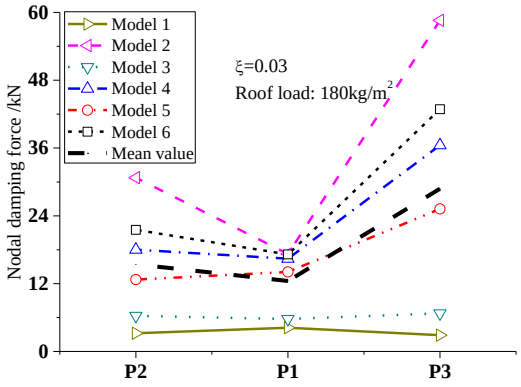

Fig. 10 Mean values of damping forces (Section A-A)

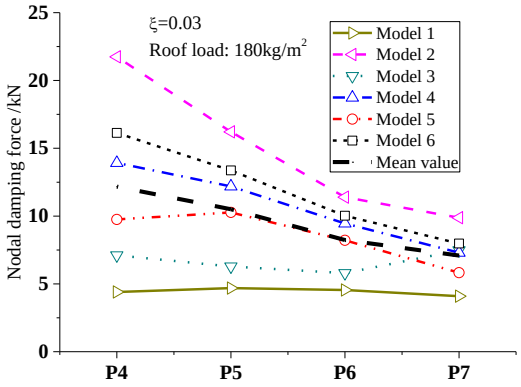

Fig. 11 Mean values of damping forces (Section B-B)

It is observed that model 1 leads to the lowest damping force, whereas the model 2 leads to the highest one. The peak viscous damping forces of the joints range from approximately 3 kN to 60 kN, and it is found that these damping force are considerably different due to the use of different damping models. Therefore, the selection of an appropriate viscous damping model is the basis for accurately predicting the viscous damping force. Based on these results, the use of model 1 may underestimate the structural damping performance, whereas model 2 may overestimate the structural damping performance. However, the results for model 5 are approximately close to the mean values of these damping models. Through a comparative analysis, it is found that the use of model 5 is a good compromise because it gives the mean damping forces in dynamic analyses, and there are no unrealistically high or low damping forces in the dome.

4.2.2 Effects of the damping ratio on the viscous damping force

Here, the effects of the different damping ratios on the damping forces of the joints are investigated. The damping ratios of 1%, 3%, and 5% are selected and the damping model 5 is used. Figs. 12 and 13 represent the vertical peak damping forces under the earthquake ground motion Victoria (Mexico, 1980). It can be seen that the damping forces of the joints increase with the increase in the damping ratio. The mean values of these damping forces are 8.8 kN (damping ratio of 1%), 14.5 kN (damping ratio of 3%), and 17 kN (damping ratio of 5%), respectively, which are approximately equal to 0.14 to 0.28 times the dead load of a joint. The vertical peak seismic force of a joint F_p can be calculated as

$$F_p = -m \times PGA_v \tag{9}$$

in which m is the mass of a joint and PGA_v is the vertical peak acceleration applied to the dome. According to the results, it is found that the vertical peak damping force is about 45%-90% of the vertical peak seismic force of a joint. It indicates that the summation of inertial force and restoring force accounts for approximately 10%-55% of total seismic force.

Moreover, it is evident that the damping force, as shown in Eq. (1), depends on not only the damping ratio but also the vibration velocity. The damping force is proportional to the damping ratio and velocity, while the increase of the damping ratio has an inhibiting effect on the velocity. Overall, however, it is observed that the damping force F_d increases with the increase in the damping ratio from Figs. 12 and 13. Therefore, it is clear that the damping ratio has a more significant effect on the damping forces as compared to the velocity.

4.2.3 Effects of the roof load on the viscous damping force

The increase in the roof load can lead to the increase in the seismic force, and the increase of mass can also change the structural dynamic characteristics, especially

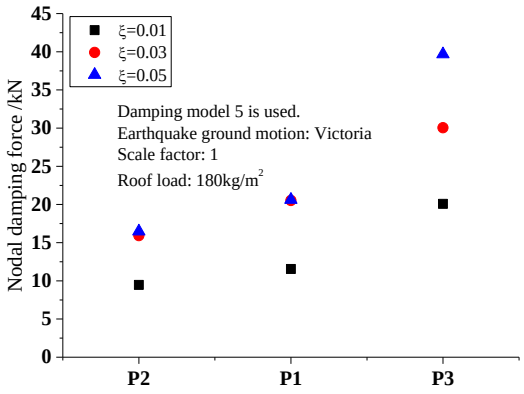

Fig. 12 Peak damping forces (Section A-A)

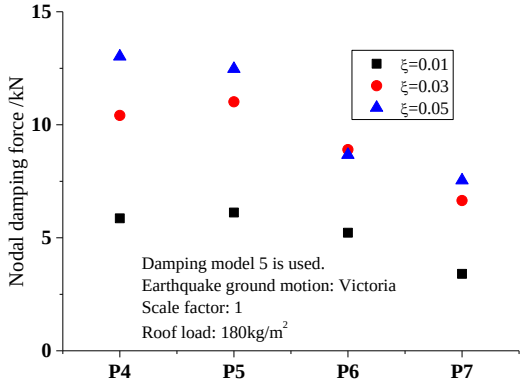

Fig. 13 Peak damping forces (Section B-B)

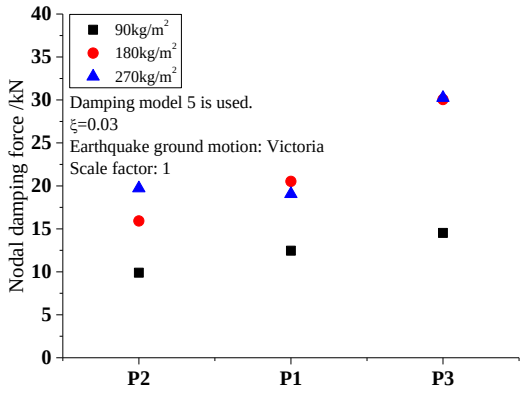

Fig. 14 Peak damping forces (Section A-A)

frequencies. It is necessary to investigate the effect of the roof load on the viscous damping force to further understand the damping performance of the dome. Figs. 14 and 15 show the vertical peak damping forces of the joints under different roof loads. The results indicate that the roof load has significant effects on these damping forces. It is found that the peak damping forces of the joints increase with the increase in the roof load. The mean values of damping forces are 8 kN (roof load of 90 kg/m^2), 14.5 kN (roof load of 180 kg/m^2), and 16 kN (roof load of 270 kg/m^2), respectively, and they are approximately equal to 0.17 to 0.26 times the dead load of a joint. The vertical peak damping force is around 50%-80% of the vertical peak seismic force of a joint. From the above analyses, it is found

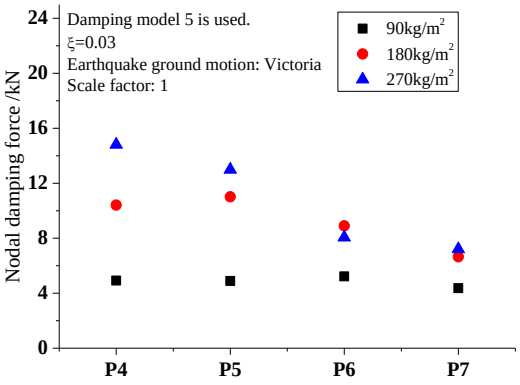

Fig. 15 Peak damping forces (Section B-B)

that the viscous damping force is an important energy dissi pation source during earthquakes and most of the energy dissipation depends on the viscous damping. However, it is difficult to accurately predict the damping forces in the dome and it should be paid more attention in engineering design.

4.3 Prediction of fatigue damage

The material fatigue damage depends on not only the intensity of earthquake but also the duration. Here, two earthquake ground motions (Tabas and Northridge) are combined in series as an earthquake excitation. After Tabas earthquake ground motion ends at 23.84s, Northridge earthquake ground motion is applied to the structure. The scale factor is set as 5 and the duration of earthquake is 63.84s.

Figs. 16 and 17 represent the cumulative fatigue damage in the mid-span sections of the elements 1 and 2 shown in Fig. 5. It is observed that the viscous damping model has a significant effect on the fatigue damage values of these sections. The effects of different damping models on the behaviors of the sections in the early cycles are limited. After a few cycles, the damage values rapidly increase. According to the analyses in Figs. 16 and 17, the model developed in the current study, which combines the R–O steel material with the fatigue effect, can describe the cumulative fatigue damage.

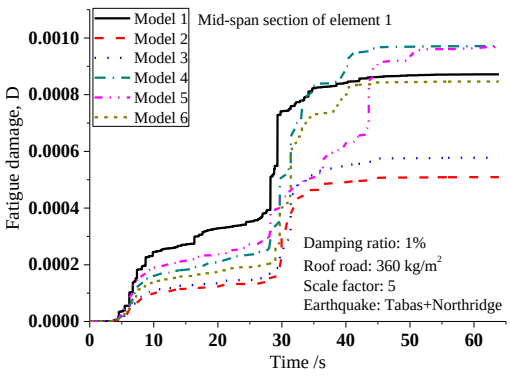

Fig. 16 Damage of mid-span section (element 1)

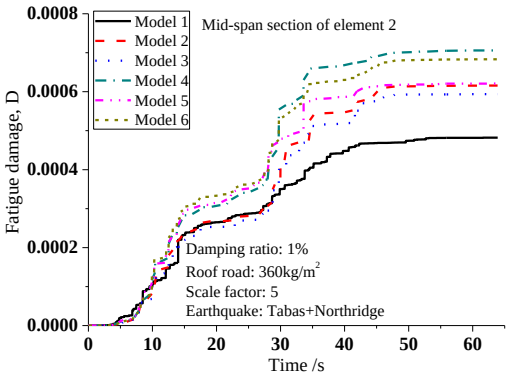

Fig. 17 Damage of mid-span section (element 2)

5. Conclusions

In the PBEE methodologies, the selection of the viscous damping model for large span single-layer latticed domes is a challenging topic for engineers because the damping cannot be accurately evaluated. Each existing damping model may have its individual limitations. As discussed in the current study, different viscous damping models have significant effects on the dynamic response, damping performance of structures, and fatigue damage of the material. Based on the above analyses and discussions, the following conclusions can be obtained:

(1) The mass-proportional damping model leads to the maximum peak response, whereas the initial stiffness-proportional damping model leads to the minimum peak response. Moreover, the initial–stiffness proportional damping model and tangent–stiffness proportional damping model approximately have the same vertical peak response. However, it should be noted that there is no shift of the modal properties between the undamaged structure and the damaged structure in the inelastic time history analysis, and those curves in Fig. 6 are only used to determine the damping coefficients α and β, which are used to construct the Rayleigh damping ($[C]=\alpha[M]+\beta[K]$).

(2) The vertical peak displacement at the top decreases with the increase in the damping ratio. The inappropriate damping ratio may not accurately predict the structural seismic performance. It should be noted that the stiffness-proportional models (models 2 and 3), Rayleigh damping model (model 4), and Hall's damping model (model 6) are more sensitive to damping ratio than the mass-proportional damping model (model 1) in inhibiting the response. The sensitivity of Charney's damping model (model 5) to the damping ratio falls in among these models.

(3) Through the analyses for the viscous damping forces in the dome subjected to earthquake ground motions, it is observed that the mass-proportional damping model leads to the lowest peak damping force, whereas the initial stiffness-proportional damping model leads to the highest one. The mean values of the peak damping forces of the joints under all the damping models are in accordance with the peak damping forces under the Charney's damping model (model 5). If the damping forces generated by the uncertain viscous damping models can be kept at an appropriate level, as a compromise, it is found that the Charney's damping model (model 5) may be a good option for a large-span single-layer latticed dome subjected to the earthquake ground motions.

(4) In the current study, the results show that the roof load and damping ratio have the significant effects on the damping forces. The peak damping forces generally increase with the increase in the roof load and damping ratio. It is also observed that the viscous damping models have a significant effect on the fatigue damage of the members.

Acknowledgments

The research described in this paper was financially supported by the National Natural Science Foundation of China (Grant No. 51108301).

References

AISC (ANSI/AISC 341-05) (2005), Seismic provisions for structural steel buildings, American Institute of Steel Construction Inc., Chicago.

Anes, V., Reis, L., Li, B. and Freitas, M. (2014), "New approach to evaluate non-proportionality in multiaxial loading conditions", *Fatigue Fract. Eng. M.*, **37**(12), 1338-1354.

ASCE/SEI 8-02 (2003), Specification for the design of cold-formed stainless steel structural members, American Society of Civil Engineers; New York, NY, USA.

ATC (1997), NEHRP Guidelines for the Seismic Rehabilitation of Buildings, Federal Emergency Management Agency, USA.

Bernal, D. (1994), "Viscous damping in inelastic structural response", *J. Struct. Eng.*, **120**(4), 1240-1254.

Charney, F.A. (2008), "Unintended consequences of modeling damping in structures", *J. Struct. Eng.*, **134**(4), 581-592.

Chopra, A.K. (1995), *Dynamics of structures*, Prentice Hall, New Jersey, USA.

CSI. (2007), Perform3D User's manual, California, USA.

Deierlein, G.G., Reinhorn, A.M. and Willford, M.R. (2010), "Nonlinear structural analysis for seismic design (NEHRP Seismic Design Technical Brief No. 4)", National Institute of Standards and Technology, U.S. Department of Commerce.

Filiatrault, A., Christopoulos, C. and Stearns, C. (2002), "Guidelines, specifications, and seismic performance characterization of nonstructural building components and equipment", Pacific Earthquake Engineering Research Center, USA.

Goel, R.K. and Chopra, A.K. (1997), "Vibration properties of buildings determined from recorded earthquake motions", Earthquake Engineering Research Center, University of California, USA.

Gupta, N.K. and Gupta, S.K. (1993), "Effect of annealing, size and cut-outs on axial collapse behavior of circular tubes", *Int. J. Mech. Sci.*, **35**(7), 597-613.

Gupta, N.K. (2004), "Experimental and numerical studies of the collapse of thin tubes under axial compression", *Lat. Am. J. Solid. Struct.*, **1**(2), 233-260.

Hall, J.F. (2006), "Problems encountered from the use (or misuse) of Rayleigh damping", *Earthq. Eng. Struct. Dyn.*, **35**(5), 525-

545.
Hindi, R.A. and Sexsmith, R.G. (2001), "A proposed damage model for RC bridge columns under cyclic loading", *Earthq. Spectra*, **17**(2), 261-290.
Jehel, P., Léger, P. and Ibrahimbegovic, A. (2014), "Initial versus tangent stiffness-based Rayleigh damping in inelastic time history seismic analyses", *Earthq. Eng. Struct. Dyn.*, **43**(3), 467-484.
Kelly, T.E. (2001), Performance based evaluation of buildings-nonlinear pushover and time history analysis-reference manual, Holmes Consulting Group, Revision 5.
Krawinkler, H. (2000), "FEMA-355 C State of the art report on systems performance of steel moment frames subject to earthquake ground shaking", Federal Emergency Management Agency, USA.
Li, Y., Wang, L., Tamura, Y. and Shen, Z. (2009), "Wind tunnel test on levy type cable dome", *The seventh asia-pacific conference on wind engineering*, Taipei, Taiwan.
Lignos, D.G., Chung, Y., Nagae, T. and Nakashima, M. (2011), "Numerical and experimental evaluation of seismic capacity of high-rise steel buildings subjected to long duration earthquakes", *Comput. Struct.*, **89**(11), 959-967.
Mazzoni, S., McKenna, F., Scott, M.H. and Fenves, G. (2004), OpenSees users manual, PEER, Berkeley, USA.
Mehanny, S.S.F. and Deierlein, G.G. (2001), "Seismic damage and collapse assessment of composite moment frames", *J. Struct. Eng.*, **127**(9), 1045-1053.
Park, Y.J. and Ang, A.H.S. (1985), "Mechanistic seismic damage model for reinforced concrete", *J. Struct. Eng.*, **111**(4), 722-739.
PEER/ATC (2010), Modeling and acceptance criteria for seismic design and analysis of tall buildings, PEER/ATC 72-1 Report; Redwood City, USA.
Ramberg, W. and Osgood, W.R. (1943), Description of stress-strain curves by three parameters, Technical Note No. 902, National Advisory Committee For Aeronautics, Washington DC, USA.
Satake, N., Suda, K. I., Arakawa, T., Sasaki, A. and Tamura, Y. (2003), "Damping evaluation using full-scale data of buildings in Japan", *J. Struct. Eng.*, **129**(4), 470-477.
Sheen, R.L. (1984), "Experimental measurement of material damping for space structures in simulated zero-G", Rept no. AFIT/CI/NR-83-84T; Air Force Inst. of Tech., Wright-Patterson AFB, OH, USA.
Shemshadian, M.E., Razavi, S.A., Hosseini, A., Mirghaderi, S.R., and Khan Mohammadi, M. (2011), "An analytical study of low cycle fatigue effects in buckling restrained braces", *3rd ECCOMAS Thematic Conference on Computational Methods in Structural Dynamics and Earthquake*, Corfu, Greece.
Stephens, R.I., Fatemi, A., Stephens, R.R. and Fuchs, H.O. (2000), *Metal fatigue in engineering*, John Wiley & Sons.
Tamura, Y. (2012), "Amplitude dependency of damping in buildings and critical tip drift ratio", *Int. J. High-Rise Build.*, **1**(1), 1-13.
Tatemichi, I., Hatato, T., Anma, Y. and Fujiwara, S. (1997), "Vibration tests on a full-size suspen-dome structure", *Int. J. Space Struct.*, **12**(3), 217-224.
Teng, J.G. (1996), "Buckling of thin shells: Recent advances and trends", *Appl. Mech. Rev.*, **49**(4), 263-274.
Uriz, P. (2005), "Towards earthquake resistant design of concentrically braced steel structures", Doctoral Dissertation, Structural Engineering, Mechanics, and Materials, Department of Civil and Environmental Engineering, University of California, Berkeley, USA.
Vargas, R. and Bruneau, M. (2007), "Effect of supplemental viscous damping on the seismic response of structural systems with metallic dampers", *J. Struct. Eng.*, **133**(10), 1434-1444.
Zareian, F. and Medina, R.A. (2010), "A practical method for proper modeling of structural damping in inelastic plane structural systems", *Comput. Struct.*, **88**(1), 45-53.
Zhang, H.D. and Han, Q.H. (2013), "A numerical investigation of seismic performance of large span single-layer latticed domes with semi-rigid joints", *Struct. Eng. Mech.*, **48**(1), 57-75.
Zhang, H.D., Han, Q.H., Wang, Y.F. and Lu, Y. (2016), "Explicit modeling of damping of a single-layer latticed dome with an isolation system subjected to earthquake ground motions", *Eng. Struct.*, **106**, 154-165.
Zhang, H.D. and Wang, Y.F. (2015), "Investigation of a joint-member damping model for single-layer latticed domes", *China Civ. Eng. J.*, **48**(2), 54-65. (in Chinese)
Zhang, H.D, Wang, Y.F. and Han, Q.H. (2015), "Nonlinear material loss factors of single-layer latticed domes subjected to earthquake ground motions", *J. Struct. Eng*., ASCE, **141**(7), 04014181.

CC